JOURNAL OF GEOPHYSICAL RESEARCH, VOL. 106, NO. A12, PAGES 29915–29924, DECEMBER 2001

Determining the mass density along magnetic field lines from toroidal eigenfrequencies: Polynomial expansion applied to CRRES data

R. E. Denton,[1] M. R. Lessard,[2] R. Anderson,[3] E. G. Miftakhova,[1] and J. W. Hughes[4]

Abstract. Because the harmonics of toroidal Alfvén wave eigenmodes have a different response to mass density at different points along a magnetic field line, the frequencies of these harmonics can, in principal, be used to infer the distribution of mass density along the field line. Here we present several improvements to the methodology and test our method using magnetic and plasma wave data from the CRRES spacecraft. Our method includes the calculation of toroidal frequencies in a Tsyganenko magnetic field assuming a polynomial expansion for the logarithm of the mass density with respect to a coordinate related to distance along the field line. We use a Monte Carlo distribution of frequencies about the observed peaks in order to infer an uncertainty for the mass density. The method only works well if the frequencies of the fundamental and second harmonic are known. We compare the inferred mass density at the spacecraft location with the electron density determined from the plasma wave experiment onboard CRRES. The observed electron density is about a factor of 2 lower than the mean of the inferred mass density for an ensemble of frequency combinations based on the uncertainties of the measured spectral peaks but is close to or within the error bars of the inferred mass density. In one of the cases examined, the inferred mass density had a local maximum at the equator, while in the other case the inferred mass density increased monotonically away from the equator.

1. Introduction

While the average properties of the equatorial plasma density in the magnetosphere have been at least approximately described [*Carpenter and Anderson*, 1992; *Gallagher et al.*, 2000], the latitudinal density dependence along field lines is less well known. Methods used to infer the latitudinal density dependence include in situ spacecraft observations and remote sensing with whistler waves and ultra low frequency toroidal alfvén frequencies [see *Goldstein et al.*, 2001, and references therein].

Magnetospheric magnetic field lines often undergo toroidal (azimuthal) Alfvén wave oscillations. Because the field lines are tied down (fixed) at the ionospheric boundary, only certain discrete frequencies are allowed; these depend on the particular harmonic, just like waves on a string. Because of the different parallel structures associated with the harmonics, the harmonic frequencies respond differently to the mass density at various locations along the field line. For instance, since the velocity perturbation of the second harmonic has a node at the equator, the frequency of the second harmonic is unaffected by a narrow peak in mass density at the equator. Because of the different response of harmonics to the mass density distribution, information about the mass density along the field line can be determined from the frequencies of the toroidal Alfvén waves [*Troitskaya and Gul'elmi*, 1967].

[1]Department of Physics and Astronomy, Dartmouth College, Hanover, New Hampshire, USA.
[2]Thayer School of Engineering, Dartmouth College, Hanover, New Hampshire, USA.
[3]Department of Physics and Astronomy, University of Iowa, Iowa City, Iowa, USA.
[4]Department of Astronomy, Boston University, Boston, Massachusetts, USA.

Paper number 2001JA000204.
0148-0227/01/2001JA000204$09.00

Most techniques to determine the dependence of mass density ρ along field lines have assumed a power law form

$$\rho = \rho_{eq}\left(\frac{LR_E}{R}\right)^{\alpha}, \tag{1}$$

where ρ_{eq} is the equatorial mass density, L is defined to be the equatorial radius in units of the Earth's radius R_E, and R is the radial distance from the center of the Earth (see references by *Menk et al.* [1999] and *Denton and Gallagher* [2000]). Assuming the power law form, *Cummings et al.* [1969] calculated toroidal eigenfrequencies at geosynchronous orbit ($L = 6.6$). *Takahashi and McPherron* [1982], *Engebretson et al.* [1986], and *Menk et al.* [1999] matched ratios of these frequencies to observed frequencies to infer values of ρ_{eq} and values of α varying from 0–6.

The method of *Price et al.* [1999] is more general in that it does not assume any particular functional dependence for the mass density. They used a finite difference approximation of the toroidal wave equation to infer the mass density at several locations along $L = 1.8$ and 2.8 magnetic field lines. As they implemented it, the method is only applicable within about $L = 3$ [*Price et al.*, 1999]; the main reason for this is that their finite difference scheme cannot accurately represent the variation in Alfvén speed due to a large variation of $R/(LR_E)$. By using higher-order differentiation, the method of *Price et al.* [1999] can be extended to arbitrarily large L [*Denton*, 2000].

In this paper, we use a Tsyganenko magnetic field model [*Tsyganenko*, 1989, 1995] as an input to the wave equation [see also *Waters et al.*, 1996; *Loto'aniu et al.*, 1999] and express the mass density in terms of a polynomial expansion in the coordinate z. (This coordinate is defined in (2); in a dipole field and in the vicinity of the equator it is proportional to the distance along a field line.) The polynomial expansion yields a somewhat more general functional dependence than the power law and seems to be able to converge better on a solution than when interpolation is used on the basis of values of ρ at fixed values of z (see section 4). By varying the frequencies of the observed harmonics about their peak values, we determine the uncertainty of the mass density. In section 2 we

describe the data we will use from the Combined Release and Radiation Effects Satellite (CRRES). In section 3 we discuss our method, and in section 4 we present our results. Using magnetic field data from the CRRES spacecraft, we infer the mass density at the spacecraft location and compare this with the electron density determined from the CRRES Plasma Wave Experiment (PWE) (the electron density can be inferred from the upper hybrid frequency noise band) [*Anderson et al.*, 1992].

There have been a number of comparisons between mass densities inferred from toroidal frequencies observed by ground magnetometers and the results of density models [*Denton and Gallagher*, 2000, and references therein]. There have been at least a couple of comparisons to electron density values inferred from whistler waves observed on the ground. *Webb et al.* [1977] found quite similar density values at $L \leq 4$ for ion density inferred from toroidal waves (using a WKB approximation for the frequencies and assuming that all ions are protons) and electron density inferred from whistler waves. *Chi et al.* [2000c] found similar temporal behavior for inferred ion and electron density.

There have also been comparisons of the mass density inferred from toroidal frequencies measured by ground magnetometers to the density measured by spacecraft. *Waters et al.* [1996] compared inferred mass density from toroidal frequencies measured with the Canadian Auroral Network for the Open Program Unified Study (CANOPUS) magnetometer array to ~1–100 eV ion densities measured by the Los Alamos geosynchronous satellite 1989-046, 4.8 hours west of CANOPUS. For one data segment the agreement was fairly good (with appropriate time shift of the data), though a precise comparison cannot be made because of the rapid time dependence coupled with the difference in local time for the two measurements (and possibly radial position as well). For a second data segment the density values from CANOPUS were at least 10 times the density detected by 1989-046. The authors appealed to heavy ions to explain the larger mass density. *Chi et al.* [2000b] also compared equatorial mass densities inferred from toroidal frequencies measured by the CANOPUS array with ion densities inferred from Los Alamos geosynchronous satellite data and found that the densities measured by the spacecraft instrument were 10–50% of the values inferred from the ground data. The time period they studied was during a storm, so a heavy ion contribution to mass density was likely. Finally, *Loto'aniu et al.* [1999] have compared mass densities inferred from CANOPUS data with plasma wave data from the CRRES spacecraft. They found excellent agreement at some times, though at other times the two densities varied by a factor of 2 or more.

In this paper we make a similar comparison between inferred mass density and electron density, but in our case we have the advantage that the magnetic fluctuations and electron density are measured at the same location. Thus our results represent an excellent test of whether we understand the values of toroidal frequencies that are observed. After making this comparison (section 4), we discuss the size of our errors in section 5 and summarize our results in section 6.

2. CRRES Data

In order to apply our methods we must measure the frequencies of several toroidal harmonics. However, these frequencies are more sensitive to the amplitude of the magnetic field B than they are to ρ, since, in general, the frequencies should depend on the Alfvén speed. (In the WKB approximation, the frequencies will be $n/(\int dl/V_A)$, where n is the harmonic number and dl is the differential length along the field line.) Therefore we choose a section of the CRRES orbit near its apogee for which the magnetic field is relatively constant. We take the magnetic field data for each orbit and do a running average of B, 40 min around each data point. We choose the data segment around the minimum of the averaged B. For the most part, the data segments we will use in this paper are for the section of data for which the running average varies only 5% from its minimum. We apply a Welsh window to the vector (unaveraged) magnetic field data for this data segment, take a Fourier transform, and get the power spectrum. Finally, we do a running average of the power spectrum over seven frequency bins.

Table 1. Data for CRRES Orbits 081 and 920

Item	Orbit 081	Orbit 920
Date	Aug. 28, 1990	Aug. 10, 1991
UT Start	0615	0008
UT End	0755	0139
R, R_E	6.21	6.46
MLAT, deg.	16.8	−7.4
MLT, hours	6.6	16.5
Dst, nT	−22	−20
p_{sw}, nPa	1.0	
$B_{y\text{-sw}}$, nT	−1.3	
$B_{z\text{-sw}}$, nT	5.3	
Kp	1.7	1.4
B Field Model[a]	T96	T89
$L = R_{max}/R_E$	7.1	6.6
z_{sc}	0.36	0.14
$B_{sc,obs}$, nT	147.	107.
$B_{sc,Tsyg}$, nT	135.	114.
$B_{eq,mod}$, nT	73.7	98.6
$n_{e-sc,obs}$, cm^{-3}	13.8 ± 1.1	8.4 ± 0.9
f_1, mHz	2.60 ± 0.4	3.8 ± 0.8
f_2, mHz	7.34 ± 0.7	7.7 ± 0.5
f_3, mHz	11.2 ± 1.0	12.2 ± 0.9
f_4, mHz	15.3 ± 0.7	16.3 ± 0.8
f_5, mHz	19.3 ± 0.7	
$\rho_{eq,S}$,[b] amu cm^{-3}	18.9 ×÷ 1.6	17.5 ×÷ 1.7
α_S	1.1 ± 3.3	4.8 ± 2.0
c_0[c]	1.64	1.17
c_2[c]	−3.37	3.29
c_4[c]	9.75	−0.61
$\rho_{sc,pol}$,[b,d] amu cm^{-3}	20. ×÷ 2.4	16. ×÷ 1.9

[a] T89 (T96) refers to the 1989 (1996) Tsyganenko magnetic field model [*Tsyganenko*, 1989, 1995].
[b] The errors here are given as a multiplicative factor (multiplied or divided rather than added or subtracted).
[c] These values are for the peak frequencies.
[d] These values are found for a distribution of frequencies about the peak frequencies with an error indicated by the width of each peak.

Initially, we selected data segments from four orbits for study. However, we eliminated two of these because the power spectra were not stationary over the entire data segment. (We may, in a future study, be able to examine the power spectra on a shorter timescale, as the lengths of the data segments we initially use are longer than necessary for this study.) The dates and start and end times of the two remaining data segments, for orbits 081 and 920, are given in Table 1. The average SM coordinates for these two data segments are also given in Table 1.

The power spectra of the local field-aligned **X**, **Y**, and **Z** components of the magnetic field (with **Z** being the magnetic field direction, $\hat{\mathbf{Y}}$ the direction of the radial vector crossed with **Z**, and $\mathbf{X} = \hat{\mathbf{Y}} \times \mathbf{Z}$) are given for orbits 081 and 920 in Figures 1 and 2, respectively. In Figure 1 the toroidal harmonics (**Y** component, indicated by the thick solid curve) are readily apparent. Our identifications of the harmonic number ($n = 1$ for the fundamental, 2 for the second harmonic, etc.) are indicated over the lines. (The index n is the number of nodes of the azimuthal magnetic fluctuation between the ionospheres.) The toroidal wave energy dominates that of the other components (except for the second harmonic at ~7 mHz, for which the poloidal power is only slightly less), so the power in these harmonics should be uncontaminated

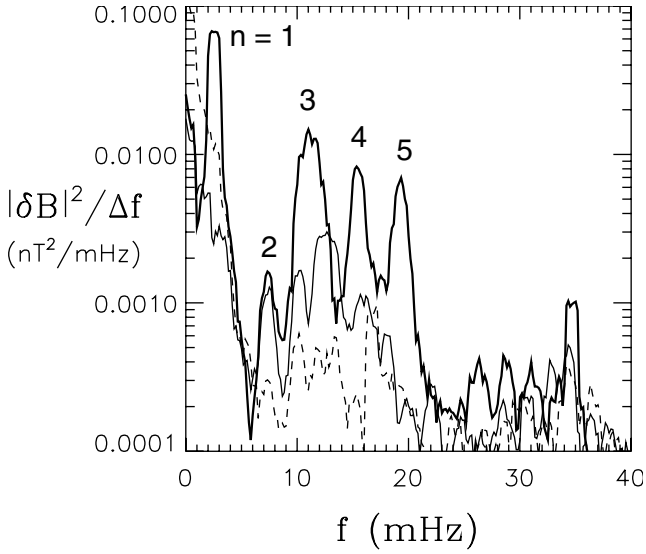

Figure 1. Power spectra for the vector components of the magnetic field for CRRES orbit 081. The vector component directions are dipole meridian **X** (thin solid curve), **Y** (bold solid curve), and **Z** (dashed curve).

by the other components. Note that the amplitude of these harmonics is very small; the amplitude of the fundamental at ~2.6 mHz is only about a third of a nanotesla. Identifying which peak corresponds to which toroidal harmonic is a nontrivial task; we will comment more on our particular identifications later. The n-dependent frequencies f_n are listed in Table 1.

It is interesting to note that the poloidal power (characterized by the **X** component) is nearly equal to the toroidal power at the second harmonic of the toroidal mode. For the poloidal mode the second harmonic is the harmonic most likely to be unstable [*Cheng and Lin*, 1987; *Chen and Hasegawa*, 1988]. The spacing of the higher-frequency poloidal harmonics (characterized by the **X** component) is less than that of their toroidal counterparts. While *Cummings et al.* [1969] found that the poloidal and toroidal frequencies were nearly equal, their calculations were for zero pressure. An inward pressure gradient can lead to reduced poloidal frequency [*Vetoulis and Chen*, 1996]. However, the simplest theory appears to lead to a greater reduction in frequency for the lower harmonics [*Vetoulis and Chen*, 1996], whereas it appears from Figure 1 that the higher harmonics may have a greater reduction in frequency.

Figure 2 shows the power spectra of the magnetic field components for CRRES orbit 920. In this case we are less sure about the frequencies of the toroidal harmonics. Note that the second harmonic is dominated by the power in the poloidal component. Nevertheless, because of the distinct peaks in toroidal power we will apply our method to this event, also.

3. Method

The wave equation for toroidal Alfvén frequencies in an arbitrary magnetic field is given by *Singer et al.* [1981]. We will use the *Tsyganenko* [1989, 1995] model [see also *Waters et al.*, 1996; *Loto'aniu et al.*, 1999]. Given the two time intervals listed in Table 1, we find the average values of *Dst* and *Kp*, the solar wind pressure p_{sw}, and the interplanetary magnetic field (IMF) components $B_{y\text{-sw}}$ and $B_{z\text{-sw}}$ as obtained from the National Space Science Data Center's (NSSDC) OMNIWeb system. These are listed in Table 1 for CRRES orbit 081; solar wind data is not available for CRRES orbit 920. We use the Tsyganenko 1996 magnetic field model for orbit 081 and the 1989 model for orbit 920 (since that model does not require the solar wind data) [*Tsyganenko*, 1989; *Tsyganenko*, 1995]. Taking into account the fact that we know the value of B at the spacecraft location $B_{sc,obs}$, we adjust the magnetic field values from the Tsyganenko model by multiplying by $B_{sc,obs}/B_{sc,Tsyg}$. In this way, we use only the shape of the field line from the model; the magnitude is determined from observation. The model value at the equator $B_{eq,mod}$ (listed in Table 1) is calculated with this adjustment. The value of $B_{sc,obs}/B_{sc,Tsyg}$ is 1.09 for orbit 081 and 0.94 for orbit 920 as can be seen from the magnetic field values listed in Table 1. Therefore the difference between observed and Tsyganenko magnetic field values is not large, and that gives some confidence about our use of the magnetic field model.

Using the wave equation of *Singer et al.* [1981], we can now calculate the toroidal frequencies if we specify the mass density along the field line. We define L as the maximum radius to any point along the field line (from the model magnetic field) divided by the Earth's radius, $L \equiv R_{max}/R_E$. For most of our calculations, the mass density distribution will be determined as a function of the coordinate z, defined as

$$z = \sqrt{1 - \frac{R}{LR_E}}. \tag{2}$$

The use of the coordinate z is suggested by the fact that in dipole coordinates, the wave equation [*Singer et al.*, 1981] separates into two terms (one with squared frequency and one with two spatial derivatives) when this spatial coordinate is used [*Radoski*, 1966]. In dipole coordinates, z is equal to the sine of the latitude from the equator, and at the equator it is proportional to the distance along the field line from the equator. However, in this paper, we will not limit ourselves to a dipole magnetic field; we consider z to be merely a convenient function of R. We will also assume that the mass density distribution is symmetric with respect to the equator ($R = R_{max} = LR_E$).

Consider, first, this functional form for the mass density:

$$\log_{10}\rho = c_0 + c_2 z^2 + c_4 z^4, \tag{3}$$

where ρ is given in amu cm^{-3}. Given a guess for the coefficients c_i, we can solve for the theoretical eigenfrequencies using a shooting code solution of the toroidal wave equation [*Singer et al.*, 1981].

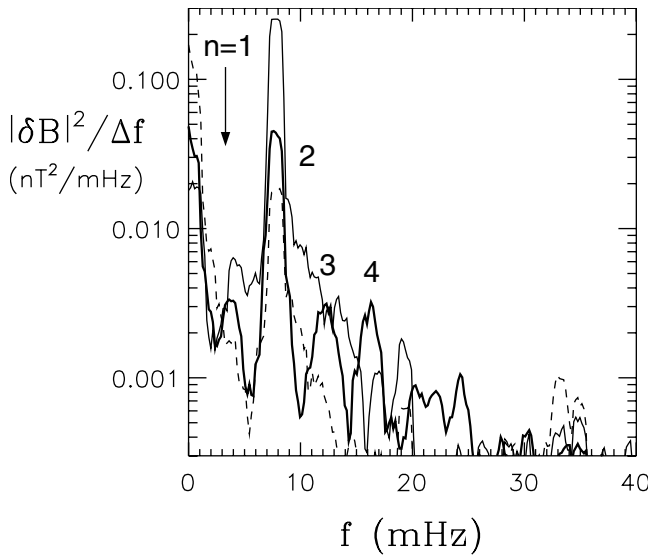

Figure 2. Power spectra for the vector components of the magnetic field for CRRES orbit 920 (same format as Figure 1).

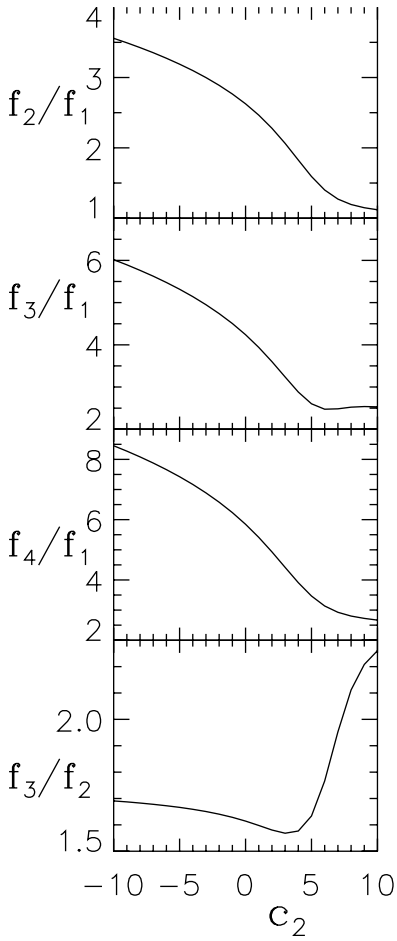

Figure 3. Ratios of the frequencies of toroidal harmonics, f_n, as a function of c_2 for mass density given by (3) if $c_4 = 0$.

Then, using a nonlinear root solver, we adjust the values of c_i until the calculated frequencies (recalculated for each adjustment of the c_i values) match the observed frequencies. We use only three frequencies at a time, and thus we have the possibility of solving for the three unknowns, c_i, from the three known frequencies. For a valid solution, we require that the calculated frequency ratios agree with the observed ratios to within 1%.

Though, in principle, one might be able to use any three frequencies, our method is much more likely to converge on a solution if one of the frequencies is the fundamental. Some understanding of this can be obtained by examining Figure 3, which plots ratios of the toroidal frequencies f_n as a function of c_2 if $c_4 = 0$. The ratio f_2/f_1 decreases monotonically with respect to c_2. So within the range of c_2 plotted here, there is a unique mapping from f_2/f_1 to c_2. (Considering our logarithmic form, (3) and the fact that z varies roughly from 0–1, $c_2 = 10$ leads to a variation in ρ of $\sim$10 orders of magnitude, so we probably do not need to consider larger values of c_2 than those shown in Figure 3.) On the other hand, f_3/f_2 has a minimum at $c_2 = 3$; some values of f_3/f_2 are consistent with two values of c_2, and some values of f_3/f_2 are not consistent with any c_2. Figure 3 indicates that we can safely calculate a value of c_2 given the frequencies of the fundamental and the second harmonic (assuming $c_4 = 0$). We have not proven that we can calculate c_2 and c_4 uniquely, given three frequencies. However, our experience is that with three frequencies we can usually converge on a solution if the three frequencies include the fundamental and the second harmonic ($n = 2$). Furthermore, when we vary the initial guess for the mass density using three frequencies, we converge on the same solution.

In order to get a guess for the initial mass density distribution we use the method of *Schulz* [1996] as implemented by *Denton and Gallagher* [2000]. (For our purposes, *Schulz* [1996] implementation would have been adequate.) This yields values of ρ_{eq} and α, assuming the power law form in (1). *Denton and Gallagher* [2000] showed that the most important feature of α in the power law form is that it determines the second derivative of the density with respect to distance along the field line or, equivalently, with respect to z (at the equator, z is proportional to distance along the field line). This is because the density in the vicinity of the equator (where B, and thus V_A, is small) has the greatest effect on the toroidal frequency. Thus for our initial mass density guess we set $c_4 = 0$ and choose c_2 such that the second derivative of ρ with respect to z is equal to that of the power law form with the values of ρ_{eq} and α inferred from *Schulz*'s [1996] method.

We use *Singer et al.*'s [1981] wave equation (9) (with a misprint in their equation corrected),

$$\frac{\partial^2}{\partial s^2}\xi' + \frac{\partial}{\partial s}(h_\alpha^2 B)\frac{\partial}{\partial s}\xi' + \frac{\omega^2}{V_A^2}\xi' = 0. \tag{4}$$

The wave function ξ' is the linear displacement in the direction of oscillation (we assumed this was the azimuthal direction) divided by h_α. The outputs of the magnetic field model which go into the solution of (4) are the distance along the field line s, the magnitude of the magnetic field B, and the displacement to an adjacent equilibrium field line h_α in the direction of oscillation. In addition, the radius R is used to relate the coordinate z to a point along the field line (with coordinate s). We assumed a perfectly conducting ionosphere at $R = 1.15\ R_E$, which means that the quantity ξ_α in Singer et al.'s equation (9) is equal to zero at that radius. Using also the evaluation of ρ along the field line as a function of s (power law form for ρ as determined from *Schulz*'s [1996] method), the eigenvalues are found using the shooting code method. Our code automatically searches up and down in frequency to get the necessary harmonics. Given our initial guess for c_2 and $c_4 = 0$, we use a globally convergent nonlinear root solver [*Press et al.*, 1997] to adjust c_2 and c_4 until the frequency ratios f_2/f_1 and f_3/f_1 match the observed values. We then adjust c_0 so that the theoretical frequencies match the observed frequencies in magnitude.

In addition to solving for the distribution of mass density if the frequencies of the harmonics are given by their peak values, we also take into account the frequency uncertainties (listed in Table 1; these are related to the half width of the peaks assuming a Gaussian shape). We generate a Monte Carlo distribution of frequencies such that the standard deviation of each harmonic about its peak value is equal to the uncertainty determined from the width of the spectral line. Then, at each value of z which is plotted, we calculate the log average of ρ and the standard deviation of $\log_{10}\rho$ for this distribution of frequencies. (As described in section 2, we have done some averaging of the power spectra displayed in Figures 1 and 2. With some fine-tuning of the method, we can reduce the uncertainty of some of the frequencies somewhat, as we show later.)

4. Results

Figure 4 shows the mass density ρ inferred by our method for the orbit 081 data as a function of z (left panel) and R/R_E (right panel). Here the functional form (3) was used for the mass density, and the frequencies f_1, f_2, and f_3 were used (where the subscript indicates the harmonic number). Concentrating first on the left panel, the middle solid curve is our solution based on the peak frequencies. The inferred values of c_0, c_2, and c_4 assuming (3) are listed in Table 1. The top and bottom solid curves represent the log average values plus and minus 1 standard deviation (in logarithm), respectively,

for an ensemble of frequencies based on the errors in frequency for the spectral lines (as described in section 3). Using (3), our code converges on a solution for ~90% of the frequency combinations (those combinations of frequencies for which there is no convergence have extreme values of the frequency ratios f_2/f_1 and f_3/f_1). Since Figure 4 is displayed with a log scale, the log average (not shown) is halfway between the top and bottom solid curves and is close to the solution based on the peak frequencies (middle solid curve) for z less than ~0.5. For z above ~0.5 the uncertainty in the result (spread between top and bottom solid curve) is very large; the most that can be said with regard to the large z values is that the mass density increases on average with respect to the ensemble of sampled frequencies.

The three diamonds in Figure 4 are plotted at values of z (and R/R_E) such that they are equally spaced with respect to the Alfvén time coordinate $\tau_A \propto \int dl/V_A\}$, where dl is the differential length along the field line and the integral is evaluated from the equator. The wave functions are more sinoidal with respect to this coordinate than with respect to other coordinates (see Figure 5), as shown by *Denton* [2000]. The quantity τ_A is normalized so that its value is unity at the ionosphere, and the values of τ_A for the three diamonds are 1/6, 3/6, and 5/6. We would not expect our solution in Figure 4 to be accurate at values of z greater than that of the right most diamond (for those values of z, variations in ρ will be overshadowed by the large variation in B), and that intuition is consistent with the large errors for $z > 0.5$.

In Figure 4 the dashed curve is the solution based on the method of *Schulz* [1996] as implemented by *Denton and Gallagher* [2000]. This method uses all five frequencies measured for orbit 081 but is based on the power law form for mass density (equation (1)) and assumes a dipole magnetic field. While the solution based on the polynomial expansion (equation (3)) yields a mass density which first decreases and then increases with respect to z, the solution based on the Schulz method is always increasing with respect to z (because of the power law form assumed it must be monotonic) but at a more moderate rate. This curve is also somewhat lower than our solution based on the Tsyganenko field (middle solid curve).

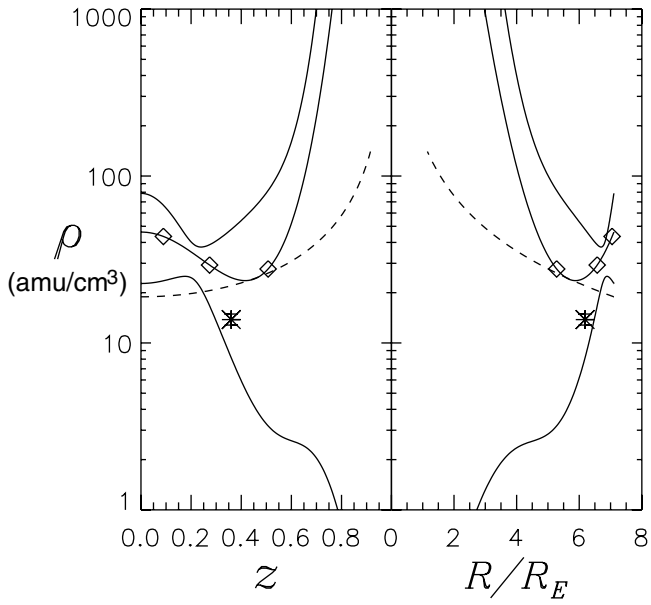

Figure 4. Mass density (in amu cm^{-3}) versus (left) z and (right) R/R_E based on the use of f_1, f_2, and f_3 for orbit 081. The middle solid curve shows our solution using the peak frequencies. The top and bottom solid curves show the log average solution for ρ plus and minus 1 standard deviation, respectively, for an ensemble of frequencies chosen so that the standard deviation of each frequency is equal to the uncertainty of the observed frequency. The dashed curve is the solution based on the method of *Schulz* [1996] as implemented by *Denton and Gallagher* [2000].

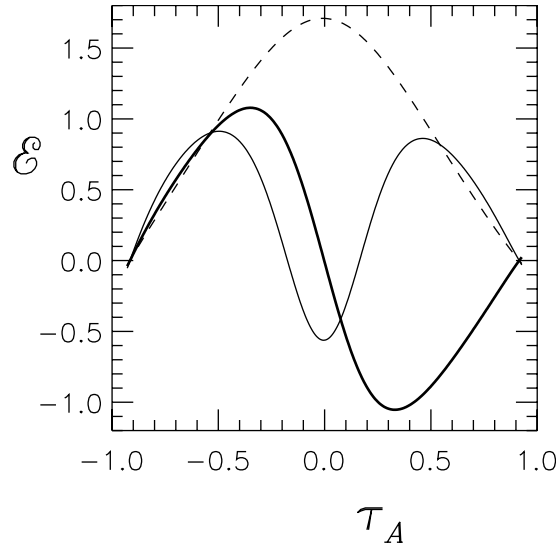

Figure 5. First three wave function solutions for $\varepsilon \equiv i\delta E_L/(\omega h_\alpha B)$ as a function of the Alfvén time coordinate τ_A.

The observed electron density at the spacecraft location based on the CRRES plasma wave data [*Anderson et al.*, 1992] ($n_{e\text{-sc,obs}}$ in Table 1) is indicated by an asterisk with error bars at the value of z corresponding to the spacecraft location z_{sc}. It is about a factor of 2 lower than the inferred mass density from our method using the peak frequencies (middle solid curve in Figure 4). Since the asterisk lies between the top and bottom solid curves, the observed electron density is within the uncertainty of our method, even neglecting the fact that the mass density may be somewhat higher than the electron density because of the possible presence of heavy ions. However, for the data segment analyzed the uncertainty of our method at the CRRES position (taking into account the width of the spectral lines) is quite large, a factor of 7; our method gives $\rho_{sc,pol} = 20. \times\div 2.4$ amu cm^{-3} (listed also in Table 1), where $\times\div$ indicates a multiplicative error (to be multiplied or divided; this arises from the logarithmic average). The right panel in Figure 4 shows that our method only gives useful information about the mass density at large values of R.

One of the interesting features of Figure 1 is that the power in the second harmonic (n=2) is much lower than that in the neighboring frequencies. If we think of CRRES as an equatorial spacecraft, we might expect that the power in the fundamental n = 1 would be the lowest. However, at the time of the orbit 081 observations the position of CRRES is significantly far from the equator with magnetic latitude (MLAT) = 16.8° (Table 1). Figure 6 shows that the CRRES position is close to a node of the second harmonic (n = 2).

We now investigate the effect of assuming a different functional form for the distribution of mass density along the field line. Here we assume a polynomial expansion for the linear mass density

$$\rho = d_0 + d_2 z^2 + d_4 z^4. \quad (5)$$

Figure 7 shows the same three solid curves as were plotted in Figure 4, except that ρ is now plotted with a linear scale. The dashed curves show the solution using the same method as was used for Figure 4, except that now ρ is expressed using (5). The two solutions using the peak frequencies (middle solid and dashed curves) are quite similar, as are the top solid and dashed curves

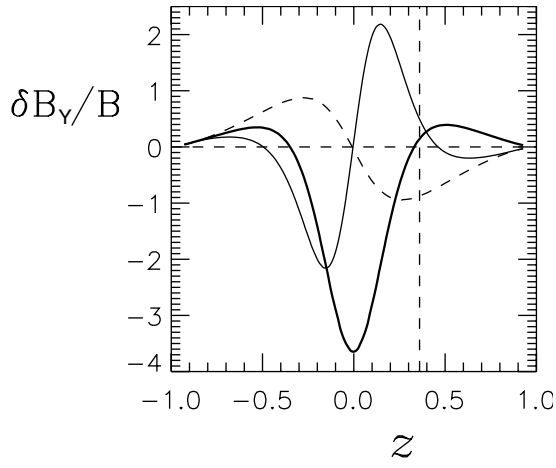

Figure 6. Azimuthal component of the perturbed magnetic field δB_y divided by the background magnetic field B as a function of z for the $n = 1$ (dashed curve), $n = 2$ (bold solid curve), and $n = 3$ (thin solid curve) eigenfunctions. The vertical dashed line is drawn at the z value corresponding to the CRRES position, and a node of the $n = 2$ eigenfunction is close to that position.

(mean plus 1 standard deviation). The bottom solid and dashed curves (mean minus 1 standard deviation) exhibit a greater difference. The bottom dashed curve has values of ρ which are negative at large values of z, whereas the solution using (3) (bottom solid curve) is constrained to positive values of ρ. (The wave equation requires only ρ, not $\sqrt{\rho}$, so we can find solutions with negative ρ.) Seeing as the negative values are unphysical, we prefer the logarithmic expansion (equation (3)).

We can also specify the mass density at several points along the field line (in a manner analogous to the method of *Price et al.* [1999]) and obtain the mass density at locations between the specified values by interpolation. We find, in general, that this method does not converge on a solution as readily as when the polynomial expansion is used. However, when both methods converge, the results are quite similar. See Appendix A for a fuller discussion.

To produce the results which were plotted in Figure 4, we used only the first three frequencies, f_1, f_2, and f_3. However, we identified five harmonics, and the frequencies of these are listed in Table 1. Unfortunately, our polynomial expansion method (using (3)) does not converge when using more than three frequencies. However, we can choose a different set of three frequencies. Figure 8 shows the results of our analysis using (3), but with f_1, f_2, and f_4 (bold dashed curve) and f_1, f_2, and f_5 (thin dashed curve). In this case, there is not a great difference between these results and those found using f_1, f_2, and f_3 (solid curves), except for large values of z for which the uncertainty in ρ is great. The frequencies f_1, f_3, and f_4 can also be used, but in that case not all frequency combinations converge on a solution; see Appendix B for a fuller description.

Now we consider the second set of data collected near the apogee of CRRES orbit 920 (see Table 1). Figure 9 shows the results of our analysis using the logarithmic polynomial expansion for ρ (3) and the set of frequencies f_1, f_2, and f_3. In this case, CRRES is closer to the equator (MLAT = −7.4°). Again, our results using the peak frequencies yield a mass density which is about a factor of 2 greater than the observed electron density, and the electron density is within the error bars found using an ensemble of frequencies based on their uncertainties. Here the range of values indicated by the error bars at the CRRES location is somewhat less than for orbit 081, about a factor of 4 ($\rho_{sc,pol} = 16. \times \div 1.9$).

The data for orbit 920 has one significant undesirable feature. This is that the toroidal power in the lower frequency harmonics (particularly for the second harmonic, $n = 2$) is less than the poloidal power (see Figure 2; the difference in the power in the two

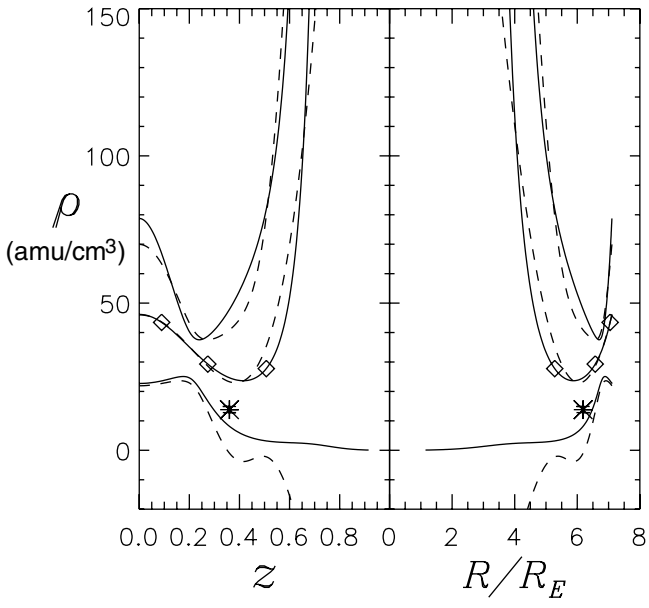

Figure 7. The three solid curves, the diamonds, and the asterisk with error bars showing the same information as was plotted in Figure 4, except that ρ is now plotted with a linear scale. The dashed curves are the corresponding solution using the linear polynomial expansion for ρ (equation (5)).

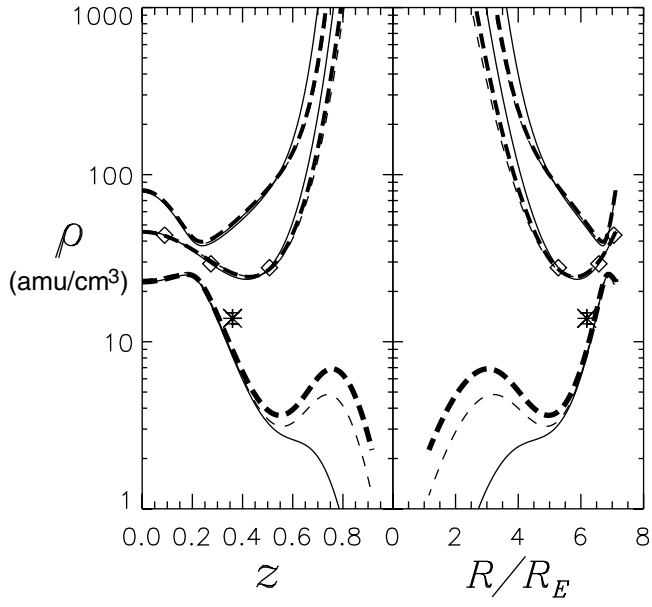

Figure 8. The solid curves, diamonds, and asterisk with error bars showing the same data as was presented in Figure 4 for orbit 081 using f_1, f_2, and f_3. The dashed curves show the corresponding solutions for the peak frequencies (middle pair of bold and thin dashed curves) and the log average plus or minus 1 standard deviation (top and bottom pairs of bold and thin dashed curves) using the same method, but with f_1, f_2, and f_4 (bold dashed curves) or f_1, f_2, and f_5 (thin dashed curves).

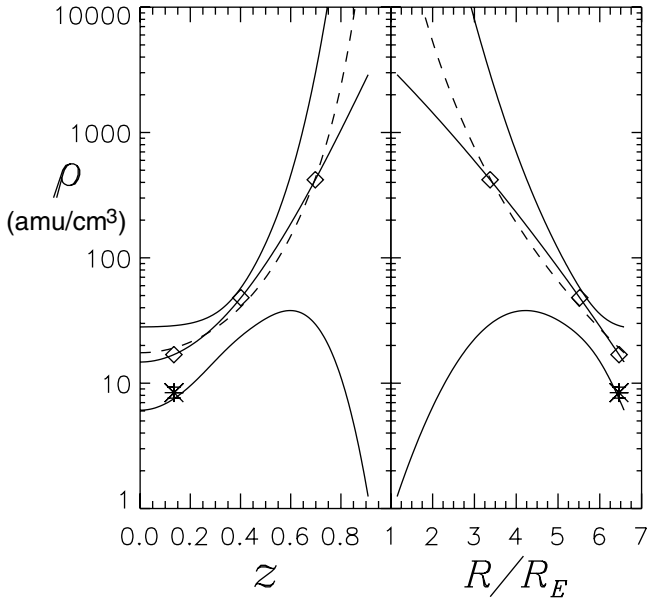

Figure 9. Same as Figure 4, except the input data is from CRRES orbit 920 (see Table 1).

components is somewhat less if we do less averaging of the power spectra with respect to frequency). In Appendix C we show results using f_1, f_3, and f_4. However, we again have the problem that the method does not converge for all frequency combinations. It appears that use of both the fundamental and second harmonic frequencies is necessary to get convergence for most frequency combinations.

5. Discussion of the Errors of the Frequencies

As was mentioned in the last paragraph of section 3, the uncertainties in frequency for the spectra lines can be reduced if a smaller time segment is used. In fact, for CRRES orbit 081 the uncertainties in frequency can be reduced by a factor of 2. In Figure 10 we show results using the logarithmic polynomial expansion with f_1, f_2, and f_3 but based on the smaller uncertainties resulting from using an hour-long segment of time. Figure 10 indicates that there really is a local maximum in mass density at the equator (the error bars in Figure 4 were so large that a flat density distribution along the field line could not be ruled out).

Unfortunately, the time segment cannot be reduced indefinitely, because there is an inherent uncertainty in the measured frequency equal to the inverse of the total amount of time. Thus, ideally, one will reduce the time segment until the uncertainty in frequency is minimized. The fact that we can reduce the uncertainty by decreasing the time segment indicates that at least part of the uncertainty in frequency is due to dependence with respect to space (sampling different flux tubes) or time. On the other hand, part of the uncertainty in frequency is likely to be due to dissipation (Q factor), which will itself give a finite width to the spectra lines. If all the spectral width were due to dissipation, it might be reasonable to take the uncertainty in frequency as the uncertainty of the peak frequency, rather than as the spectra width. This would yield significantly lower uncertainties. Further examination of how the uncertainties in frequency change with respect to length of the time segment is desirable in order to try to ascertain how much of the spectral width is due to space or time dependence, and how much is due to dissipation. Even if the spectral widths are entirely due to space or time dependence, one might argue that the individual frequencies are correlated, leading to a lower uncertainty (M. Engebretson, private communication, 2001).

6. Summary

Toroidal Alfvén frequencies can be used to infer the distribution of mass density along magnetic field lines. Here we have developed the methodology and tested our method using data from the CRRES spacecraft. This work is important for two reasons. First of all, inferring mass density along field lines using toroidal Alfvén frequencies is a promising technique to remotely sense the magnetosphere using ground-based data [*Waters et al.*, 1996; *Menk et al.*, 1999; *Loto'aniu et al.*, 1999; *Chi et al.*, 2000a]. Secondly, the toroidal Alfvén mode is one of the most fundamental waves in the magnetosphere. It is important to see if we understand how to calculate it correctly.

Our method only works well if both the fundamental and second harmonic frequencies are measured. The functional form which worked best in our code was a polynomial expansion of the logarithm of the mass density with respect to the coordinate z (equation (2) ; probably the method would work just as well using the distance along the field line s).

Using magnetic field data, we were able to identify at least five harmonics of the toroidal Alfvén wave in one case (orbit 081). However, with our method we were only able to use three frequencies at a time in the analysis. It would be advantageous to use all the frequencies in order to get all the information that we possibly can. One possible improvement of our method is to drop the assumption that the derivative of the mass density with respect to distance along the field line is zero at the magnetic equator. Asymmetry in the magnetic field could possibly lead to asymmetry in the mass density, and at this point it is unclear what the effect would be on the mass density solution if symmetry about the equator is assumed when the true solution is asymmetric. Our equations assume a perfectly conducting ionosphere

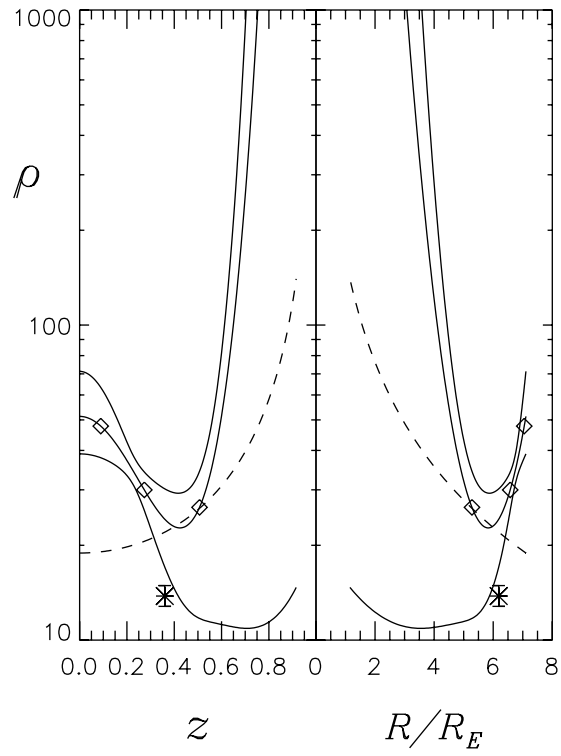

Figure 10. Same as Figure 4 but based on reduced uncertainties for frequency which result from using a smaller time segment.

at both boundaries. *Southwood and Kivelson* [2001] have recently demonstrated that differing ionospheric conductivity at the two ionospheres can result in asymmetry in the wave solutions; the results of such asymmetry should also be investigated. Another possible improvement of the interpolation method is to allow the interpolation points to float to different positions as the code converges on a solution.

If the uncertainties in frequency are large, the uncertainty in the inferred mass density can also be quite large. We have outlined a procedure to estimate the error in mass density using an ensemble of frequency combinations based on the uncertainties of the individual frequencies. In the case of the data analyzed in this paper, the range of values for mass density at the spacecraft position (within 1 standard deviation of the mean logarithmic value) varied by a factor of 7 in one case (orbit 081) and by a factor of 4 in the other (orbit 920). On the other hand, we showed that these errors could be reduced if a shorter time segment was used.

One interesting result of this paper is that in one case (CRRES orbit 081), our results indicate that the mass density has a local maximum at the equator. Some observations have indicated that the density may be peaked at the equator [*Gallagher et al.*, 2000]. Such a situation could develop from "top-down" refilling from shock formation at the equator [*Singh and Horwitz*, 1992], though the processes involved in refilling have yet to be confirmed (D. Gallagher, private communication, 2001).

Clearly, frequencies must be measured as accurately as possible in order to accurately infer mass density. We have limited ourselves to the magnetic field data. Possibly, by combining electric and magnetic field data, we can determine the frequencies with greater accuracy. Using the electric field data would also help in the identification of the harmonics (which is necessary before our method can be applied). If we can justify the assumption that most of the width of the spectral lines is due to dissipation (see discussion in section 5), the errors in frequency might be less than we have indicated.

In the case of both data segments studied here, the observed electron density (based on the plasma wave data) is lower than the mean mass density (the mean value based on an ensemble of frequencies) by about a factor of 2 (though it is close to or within the range of error). The mass density model of *Gallagher et al.* [2000] (based in part upon the work of *Craven et al.* [1997]) has the mass density ~15% larger than the electron density, not enough to explain a factor of 2 difference in the densities. During storm times the ratio of mass density to electron density would be expected to be higher, but *Dst* is not particularly large for these events (about −20 as can be seen from Table 1). It would be worthwhile to examine heavy ion data gathered by the low-energy magnetospheric ion composition sensor instrument [*Young et al.*, 1992] on the CRRES spacecraft to get a better measurement of the mass density at the spacecraft location. This would provide an even better test of the method.

Appendix A: Linear Interpolation Method Applied to CRRES Orbit 081

Figure A1 shows the results that we get for CRRES orbit 081 if we specify the mass density at three points and interpolate to positions between those points. The three positions which we choose correspond to $\tau_A = 0$, 1/3, and 2/3. The interpolation we use is quadratic with respect to position s (with zero slope at $s = 0$) between the two positions corresponding to $\tau_A = 0$ and $\tau_A = 1/3$, and linear with respect to s between the positions corresponding to $\tau_A = 1/3$ and $\tau_A = 2/3$. Beyond $\tau_A = 2/3$, ρ is linearly extrapolated with the same slope as was used for the region between $\tau_A = 1/3$ and $\tau_A = 2/3$. The evaluation of the z and s values (length along field line) corresponding to these τ_A values

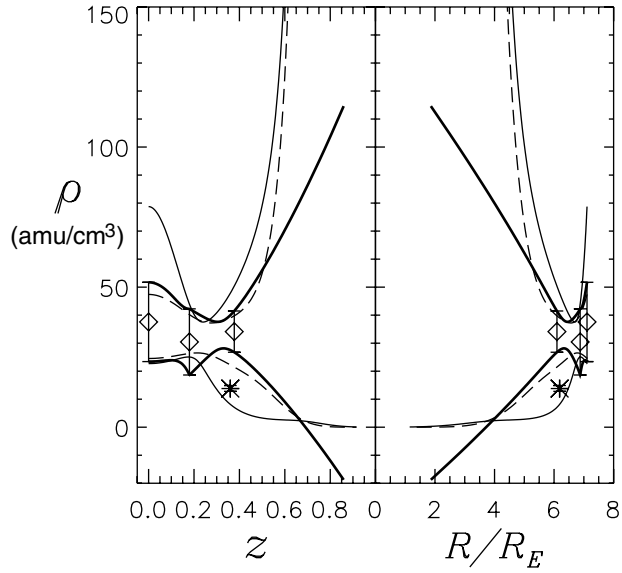

Figure A1. Solution for ρ for orbit 081 using interpolation between ρ values specified at three positions corresponding to τ_A = 0, 1/3, and 2/3. The diamonds with error bars indicate the solution at these positions. The bold solid curves represent the interpolated values of the mean plus and minus 1 standard deviation. The thin solid curves and asterisk with error bars are the same as were plotted in Figure 4. The dashed curve is described in the text.

is performed using the mass density based on the *Schulz* [1996] method. Figure 5 shows the wave eigenfunctions versus τ_A for our solution using the logarithmic polynomial expansion (3) (middle curve in Figure 4). The value $\tau_A = 0$ corresponds to a node of the second harmonic ($n = 2$), $\tau_A = 1/3$ corresponds to a position which is close to a node for the third harmonic ($n = 3$), and $\tau_A = 2/3$ corresponds to a position where all the eigenfunctions are significantly nonzero. On the basis of these facts we might expect our method to converge on a solution. However, there are many combinations of frequencies within the error bars of the spectral lines for which our code does not converge on a solution (see also *Price et al.* [1999] for whom some frequency combinations did not yield a solution). (This situation might be improved somewhat if we reevaluated the mapping from z and s to τ_A for each set of frequencies; we have based the mapping on the peak frequencies only.)

Figure A2 shows the combinations of frequency ratios, f_2/f_1 and f_3/f_1 for which our method using interpolation converges (diamonds) and for which it does not converge (dots). The vertical and horizontal lines indicate the frequency ratios for the peak values of the spectral lines. Note that the total distribution of frequencies (diamonds and dots) is elongated toward the top right and bottom left; this is due to the fact that changes in f_1 have the same effect on f_2/f_1 and f_3/f_1. Figure A2 shows that our interpolation method is more likely to converge, in this case, for smaller values of f_2/f_1.

In Figure A1 the diamonds with error bars indicate the solution at the three positions corresponding to τ_A = 0, 1/3, and 2/3 using the interpolation method. The bold solid curves represent the interpolated values of the mean plus or minus 1 standard deviation, while the top and bottom thin solid curves and asterisks with error bars are the data as were plotted in Figure 4 (resulting from our solution with the logarithmic polynomial expansion (3)). On the basis of these curves the interpolation method appears to lead to a more constrained value

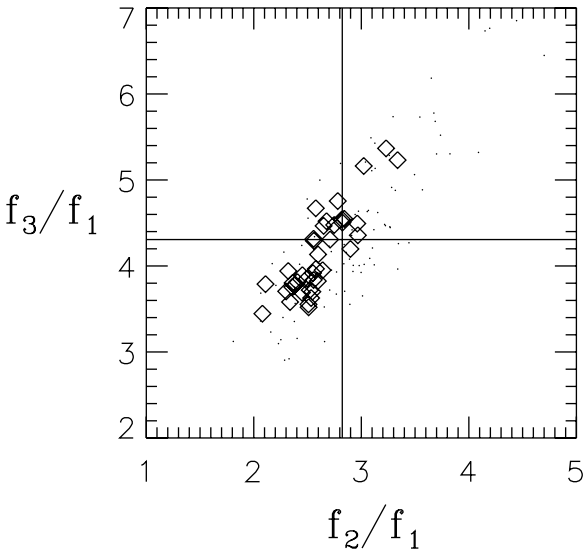

Figure A2. Values of f_2/f_1 versus f_3/f_1 for which our method using interpolation converges (diamonds) and for which it does not converge (dots). The vertical and horizontal lines indicate the frequency ratios for the peak values of the spectral lines (orbit 081).

of ρ. For instance, the error bars for $\tau_A = 2/3$ (at a z value close to that of CRRES as indicated by the asterisk) are much smaller than those resulting from the logarithmic polynomial expansion. However, we must keep in mind that the frequency set is not the same. If we rerun our code using the logarithmic polynomial expansion but use only those combinations of frequency for which the linear interpolation method converged, the resulting values of ρ for log average mean plus and minus 1 standard deviation are given by the dashed curves in Figure A1. These dashed curves are very close to the corresponding bold curves which result from a linear interpolation method. Therefore the difference in the interpolation results and the logarithmic polynomial expansion results are mainly due to the difference in frequency set.

It is not too surprising that the interpolation method as we have implemented it has trouble converging on a solution for some frequency combinations. The interpolation method allows for local minima and maxima of ρ, but these local minima and maxima must occur at the locations of the interpolation points ($\tau_A = 0$, 1/3, and 2/3). While another method (e.g., cubic spline interpolation) would allow for local minima and maxima at different locations, our experience is that such methods have even a lower percentage of convergence.

Appendix B: Logarithmic Polynomial Expansion Method Using f_1, f_3, and f_4 Applied to CRRES Orbit 081

The results shown in Figure B1 are based on the logarithmic polynomial expansion for ρ (equation (3)), using f_1, f_3, and f_4 (dashed curves). The results are similar to those using f_1, f_2, and f_3 (solid curves, equivalent to solid curves in Figure 4), but there is a greater difference here than was evident in Figure 8. However, the analysis using f_1, f_3, and f_4 suffers from the same problem that we had using the linear interpolation method (leading to Figure A1 in Appendix A). When using f_1, f_3, and f_4, our code converges on a solution for only about two thirds of the frequency combinations in the ensemble determined by the uncertainties of the spectral peaks. Thus the results shown in Figure B1 are not representative of the entire distribution of frequencies.

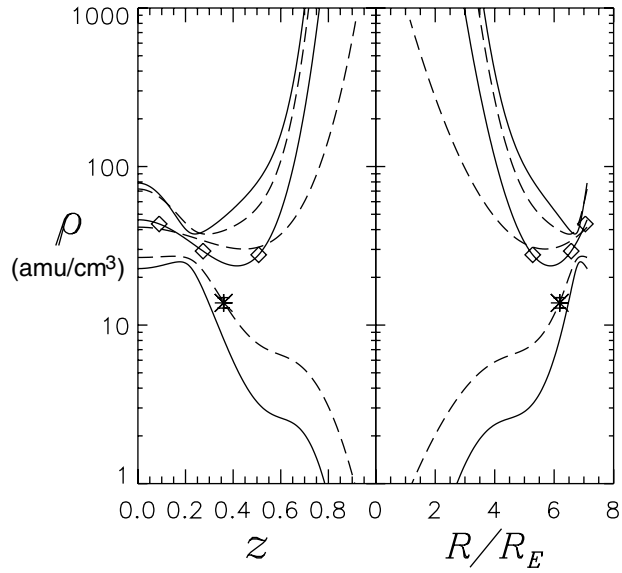

Figure B1. Same as Figure 8 except that there is only one set of dashed curves which corresponds to the frequency set f_1, f_3, and f_4.

Appendix C: Logarithmic Polynomial Expansion Method Using f_1, f_3, and f_4 Applied to CRRES Orbit 920

The results shown in Figure C1 are for orbit 920 using the logarithmic polynomial expansion for ρ (equation (3)). The three solid curves, diamonds, and asterisks with error bars are the same as were plotted in Figure 9, based on the analysis of f_1, f_2, and f_3. The dashed curves result from the same analysis but using f_1, f_3,

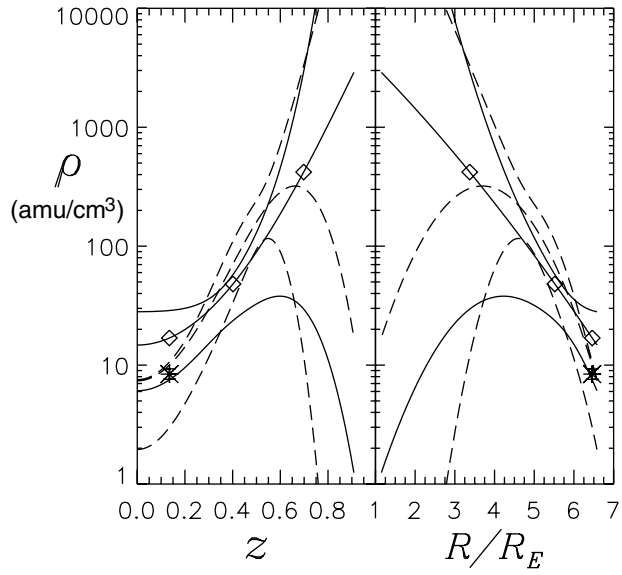

Figure C1. The three solid curves, diamonds, and asterisks with error bars are the same as were plotted in Figure 9, based on the analysis of f_1, f_2, and f_3. The dashed curves result from the same analysis but using f_1, f_3, and f_4.

and f_4. The observed electron density $n_{e\text{-sc,obs}}$ is within the range of the error bars for both runs; however, when f_1, f_2, and f_3 are used, $n_{e\text{-sc,obs}}$ is near the bottom of the range of ρ values, whereas when f_1, f_3, and f_4 are used, $n_{e\text{-sc,obs}}$ is near the top of the range. While our code using f_1, f_2, and f_3 converged for more than 90% of the frequency combinations within the uncertainties of the spectral lines, when f_1, f_3, and f_4 were used, the code converged on a solution for only ~55% of the frequency combinations. Therefore the results using f_1, f_2, and f_3 (Figure 9) are more representative of the entire distribution of frequencies.

Acknowledgments. This work was supported by NASA grants NAG5-8441, NAG5-7442, and NAG5-7803 (MRL), and NSF grant ATM-9911975. We thank NSSDC for making the IMP 8 solar wind, *Dst* (Kyoto University), and *Kp* (NOAA) data available on OMNIWeb.

Janet G. Luhmann thanks Erling Nielsen and Dennis L. Gallagher for their assistance in evaluating this paper.

References

Anderson, R. R., D. A. Gurnett, and D. L. Odem, CRRES plasma wave experiment, *J. Spacecr. Rockets*, *29*, 570, 1992.

Carpenter, D. L., and R. R. Anderson, An ISEE/whistler model of equatorial electron density in the magnetosphere, *J. Geophys. Res.*, *97*, 1097, 1992.

Chen, L., and A. Hasegawa, On magnetospheric hydromagnetic waves excited by energetic ring current particles, *J. Geophys. Res.*, *93*, 8763, 1988.

Cheng, C. Z., and C. S. Lin, Eigenmode analysis of compressional waves in the magnetosphere, *Geophys. Res. Lett.*, *14*, 884, 1987.

Chi, P. J., C. T. Russell, S. Musman, W. K. Peterson, G. Le, V. Angelopoulos, G. D. Reeves, M. B. Moldwin, and F. K. Chun, Plasmaspheric depletion and refilling associated with the September 25, 1998, magnetic storm observed by ground magnetometers at L = 2 , *Geophys. Res. Lett.*, *27*, 633, 2000a.

Chi, P. J., C. T. Russell, M. F. Thomsen, W. K. Peterson, and S. M. Petrinec, Multi-point observations of the magnetospheric plasma density during the September 1998 magnetic storm, *EOS Trans. AGU*, *81*(19), Spring Meet. Suppl., Abstract no. SM52B-06, 2000b.

Chi, P. J., C. T. Russell, D. L. Carpenter, H. Kawano, and K. Yumoto, Plasmaspheric dynamics explored by ground observations of ULF and VLF waves, *EOS Trans. AGU*, *81*(48), Fall Meet. Suppl., Abstract no. SM21B-03, 2000c.

Craven, P. D., D. L. Gallagher, and R. H. Comfort, Relative concentration of He+ in the inner magnetosphere as observed by the DE 1 retarding ion mass spectrometer, *J. Geophys. Res.*, *102*, 2279, 1997.

Cummings, W. D., R. J. O'Sullivan, and P. J. Coleman, Jr., Standing Alfvén waves in the magnetosphere, *J. Geophys. Res.*, *74*, 778, 1969.

Denton, R. E., Determining the mass density dependence along field lines using toroidal Alfvén frequencies, *EOS Trans. AGU*, *81*(19), Spring Meet. Suppl., Abstract no. SM42C-05, 2000.

Denton, R. E., and D. L. Gallagher, Determining the mass density along magnetic field lines from toroidal eigenfrequencies, *J. Geophys. Res.*, *105*, 27,717, 2000.

Engebretson, M. J., L. J. Zanetti, and T. A. Potemra, Harmonically structured ULF pulsations observed by the AMPTE CCE magnetic field experiment, *Geophys. Res. Lett.*, *13*, 905, 1986.

Gallagher, D. L., P. D. Craven, and R. H. Comfort, Global core plasma model, *J. Geophys. Res.*, *105*, 18,819, 2000.

Goldstein, J., R. E. Denton, M. K. Hudson, E. G. Miftakhova, S. L. Young, J. D. Menietti, and D. L. Gallagher, Latitudinal density dependence of magnetic field lines inferred from Polar plasma wave data, *J. Geophys. Res.*, *106*, 6195, 2001.

Loto'aniu, T. M., C. L. Waters, B. J. Fraser, and J.-C. Samson, Plasma mass density in the plasmatrough: Comparison using ULF waves and CRRES, *Geophys. Res. Lett.*, *26*, 3277, 1999.

Menk, F. W., D. Orr, M. A. Clilverd, A. J. Smith, C. L. Waters, D. K. Milling, and B. J. Fraser, Monitoring spatial and temporal variations in the dayside plasmasphere using geomagnetic field line resonances, *J. Geophys. Res.*, *104*, 19,955, 1999.

Press, W. H., S. A. Teukolsky, W. T. Vetterling, and B. P. Flannery, *Numerical Recipes in Fortran 77: The Art of Scientific Computing vol. 1, Fortran Numer. Recipes*, 994 pp., Cambridge Univ. Press, New York, 1997.

Price, I. A., C. L. Waters, F. W. Menk, G. J. Bailey, and B. J. Fraser, A technique to investigate plasma mass density in the topside ionosphere using ULF waves, *J. Geophys. Res.*, *104*, 12,723, 1999.

Radoski, H. R., Magnetic toroidal resonances and vibrating field lines, *J. Geophys. Res.*, *71*, 11,891, 1966.

Schulz, M., Eigenfrequencies of geomagnetic field lines and implications for plasma-density modeling, *J. Geophys. Res.*, *101*, 17,385, 1996.

Singer, H. J., D. J. Southwood, R. J. Walker, and M. G. Kivelson, Alfven wave resonances in a realistic magnetospheric magnetic field geometry, *J. Geophys. Res.*, *86*, 4589, 1981.

Singh, N., and J. L. Horwitz, Plasmasphere refilling: Recent observations and modeling, *J. Geophys. Res.*, *97*, 1049, 1992.

Southwood, D. J., and M. G. Kivelson, Damping standing Alfvén waves in the magnetosphere, *J. Geophys. Res.*, *106*, 10,829, 2001.

Takahashi, K., and R. L. McPherron, Harmonic structure of Pc 3–4 pulsations, *J. Geophys. Res.*, *87*, 1504, 1982.

Troitskaya, V. A., and A. V. Gul'elmi, Geomagnetic micropulsations and diagnostics of the magnetosphere, *Space Sci. Rev.*, *7*, 689, 1967.

Tsyganenko, N. A., A magnetospheric magnetic field model with a warped tail current sheet, *Planet. Space Sci.*, *37*, 5, 1989.

Tsyganenko, N. A., Modeling the Earth's magnetospheric magnetic-field confined within a realistic magnetopause, *J. Geophys. Res.*, *100*, 5599, 1995.

Vetoulis, G., and L. Chen, Kinetic theory of geomagnetic pulsations, 3, Global analysis of drift Alfvén ballooning modes, *J. Geophys. Res.*, *101*, 15,441, 1996.

Waters, C. L., J. C. Samson, and E. F. Donovan, Variation of plasmatrough density derived from magnetospheric field line resonances, *J. Geophys. Res.*, *101*, 24,737, 1996.

Webb, D. C., L. J. Lanzerotti, and C. G. Park, A comparison of ULF and VLF measurements of magnetospheric cold plasma densities, *J. Geophys. Res.*, *82*, 5063, 1977.

Young, D. T., B. L. Barraclough, D. J. McComas, M. F. Thomsen, K. McCabe, and R. Vigil, CRRES low-energy magnetospheric ion composition sensor, *J. Spacecr. Rockets*, *29*, 596, 1992.

R. Anderson, Department of Physics and Astronomy, 615 Van Allen Hall, University of Iowa, Iowa City, IA 52242, USA.

R. E. Denton and E. G. Miftakhova, Department of Physics and Astronomy, 6127 Wilder Laboratory, Dartmouth College, Hanover, NH 03755, USA. (richard.denton@dartmouth.edu)

J. W. Hughes, Boston University, Department of Astronomy, 725 Commonwealth Avenue, Boston, MA 02215, USA.

M. R. Lessard, Thayer School of Engineering, HB 8000, Dartmouth College, Hanover, NH 03755, USA.

(Received July 6, 2001; revised August 21, 2001;
accepted August 21, 2001.)